European Battery, Hybrid and Fuel Cell Electric Vehicle Congress
Brussels, Belgium, December 1-4, 2015

Aging Inhomogeneity influenced by Cell Size in Commercial Pouch Cells

Raghavendra Arunachala[1], Lemuel Moraleja[1], Andreas Jossen[2], Juergen Garche[3]
[1]*TUM CREATE Ltd Singapore, 1 Create Way 10-02 Create Tower*
raghavendra.arunachala@tum-create.edu.sg
[2]*Institute for Electrical Energy Storage Technology, Technische Universität München (TUM)*
[3]*Fuel Cell and Battery Consulting FCBAT Ulm, Germany*

Abstract

Large format cells are becoming popular choice for electric vehicle (EV) applications; as they are being made available by commercial cell manufacturers. Recent studies show that increase in the cell size introduces inhomogeneity to the cells in the form of current density, temperature and state of charge (SOC) distribution. These inhomogeneities lead to non-uniform aging within the cell. The contemporary researches on aging studies are mainly focused on influence of temperature, current rate (c-rate), operating voltage, SOC swing etc. This paper is aimed to study aging characterization of commercial lithium ion cells of nickel manganese cobalt oxide (NMC) chemistry by comparing different sizes of 8 Ah, 25 Ah, 53 Ah and 75 Ah cell capacities respectively. Since the inhomogeneities mainly come from cycling, the cycle life is in the focus of our investigations. But also, a comparison was made between calendar aging and cycle aging of these cells at 40°C ambient temperature. Our theoretical calculations are made based on finite element method (FEM) modeling in COMSOL Multiphysics platform to evaluate inhomogeneity within the cell.

Keywords: large format cells, cell size, spatial inhomogeneity, inhomogeneous aging

1 Introduction

Lithium ion battery is the most preferred choice for electrical energy storage systems due to its high energy density, high power density, long cycle life and low self-discharge. They are widely used in many portable applications such as, cell phones, digital cameras, laptops and other electronics. They are popular choice for green transportation such as, electric vehicles (EVs) and hybrid electric vehicles (HEVs) and other forms of electromobility [1].

However, like in many other battery systems, lithium ion batteries suffer from capacity loss and power loss, which can be described by aging mechanism in the cell. Aging is a complex process occurring due to electrochemical changes as consequences of structural and mechanical changes of all the cell components. It is characterized by deterioration of battery performance with time and usage. According to this definition, it can be classified into calendar aging (calendar life or shelf life of the cell [2]) and cycle aging (cycle life).

In private EVs, with about 90% of rest time, the calendar aging determines the lifetime of the battery [3]. Calendar aging is described in several literature sources. It is known that the formation of solid electrolyte interphase (SEI) with the passage of time leads to consumption of cyclable lithium ions and increase in the cell impedance [4, 5].

The SEI formations is aslo the main reason for cycle aging. Additionally, lithium plating, secondary losses such as degradation of active materials, decomposition of binders, loss of contact between current collector and active material due to volume changes during cycling are

taken into account. These effects are well documented in literature with extensive studies on different temperatures, c-rates, operating voltage, cell chemistries etc. [6–8].
Besides, these microscopic changes that influences cycle aging, some macroscopic effects such as, cell form, geometry, tab size and location, thicknesses of active materials, separator and current collectors and cell size also influences the performance and aging of large format cells. E.g. the increase of the thickness of active materials leads to on the one hand to an improved energy density and material utilization of a cell, but it also increases the mean diffusion path of the ions thereby increasing the polarization and reducing the material utilization. Furthermore the higher energy leads to higher safety risk. Increase in the thickness of the current collector improves the conductivity of current and minimizes the cell internal resistance, but it contributes to the dead weight of the cell resulting in lower energy density. Therefore an optimal cell design has to be considered not only with respect to energy but also with respect to power and safety of the cell, i.e. it has to balance the active materials, current collectors and separator for a given application.
The current distribution in the cell is affected by the design of tab size, location and aspect ratio of the cell, besides the current collector thickness. In spite of optimal designs, the current flow near the tabs is constricted, which causes the location near the tabs to experience higher current density and influences the local SOC [9, 10]. This phenomenon contributes to increase in local heat generation of the cell and hence the temperature rise. As a result, there is an inhomogeneous distribution of temperature, SOC and current along the plane of the cell. In general the temperature inhomogeneity is also contributed by surface area to volume ratio of the cell. A low ratio leads to larger temperature inhomogeneity and vice versa. These inhomogeneous cell characteristics could lead to non-uniform aging in the cell as shown in Fig.1.

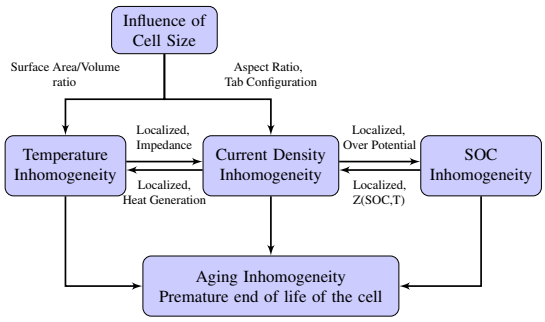

Figure 1: Schematic of aging inhomogeneity and its influencing factors

Extensive research on cell inhomogeneity shows that, it occurs during different cycling conditions and hence they are not affected by storage conditions [11, 12]. This paper presents the influence of cell size (8, 25, 53 and 75 Ah cells) on the aging. The cells were chosen from the same commercial manufacturer for the reason of superior manufacturing process and reproducibility of results. The cell chemistries were same as described the datasheets of the manufacturer. Other microscopic parameters such as active material, separator and current collector thicknesses we found to be in the same range with $\pm 2\%$ variations. Each cell type was performed with calendar and cycle aging (on separate cells) at 40°C ambient conditions.

2 Experimental

The experimental investigations were performed on high energy lithium ion pouch cells. The nominal voltage of these cells were 3.7 V. The active material consists of lithium nickel manganese cobalt oxide as cathode, graphite as anode and $LiPF_6$ blended with ethylene carbonate (EC) and ethyl methyl carbonate (ECM) as electrolyte material. Other specifications of the investigated cells are shown in Tab. 1.

Table 1: Specification of investigated cells

Nominal Capacity (Ah)	Size (mm) (WxHxT)	Weight (g)	Electrode Area Ratio (Cathode/Anode)	No. of layers
8	$105 \times 100 \times 7.05$	157	0.952	16
25	$225 \times 224 \times 6$	570	0.963	14
53	$225 \times 224 \times 12.3$	1,200	0.965	29
75	$263 \times 266 \times 11.2$	1,500	0.983	28

The investigations of aging inhomogeneity with the influence of sizing were based on the literature inputs. In general cell inhomogeneity is influenced by ambient temperature and c-rates. Low ambient temperature and high c-rates lead to higher degree of inhomogeneity in the cell and vice versa [13]. At first, the cells were discharged at different c-rates 0.5, 1, 2 and 3C using a battery tester (Digatron MCT), at temperatures 15, 25 and 40°C inside the climate chamber (ESPEC PU-3J). In addition to this, several temperature sensors (thermo-couple t-type) were placed on cells during the tests to measure its spatial temperature distribution with the help of a datalogger (Agilent 34980A Multiswitch). After the conclusion of the tests, temperature gradients were calculated for each discharge c-rate and temperature.
Fig.2 shows the maximum surface temperature gradient (ΔT) measured on different cell sizes at various temperatures and c-rates. These results are in agreement with the literature sources, besides ΔT is also influenced by the cell size. Cycling at low ambient temperature (15°C) and/or with high discharge c-rate (3C) would make a perfect case to study aging inhomogeneity. But these conditions are also favourable for lithium plating, another aging process occurring in the cell. Since this aging inhomogeneity study is based on influence of sizing under the pretext of cell geometry, 40°C and 1C cycling (charge and discharge) conditions were preferred for cycle aging. The ambient temperature 40°C was chosen for another reason, i.e. to compare the re-

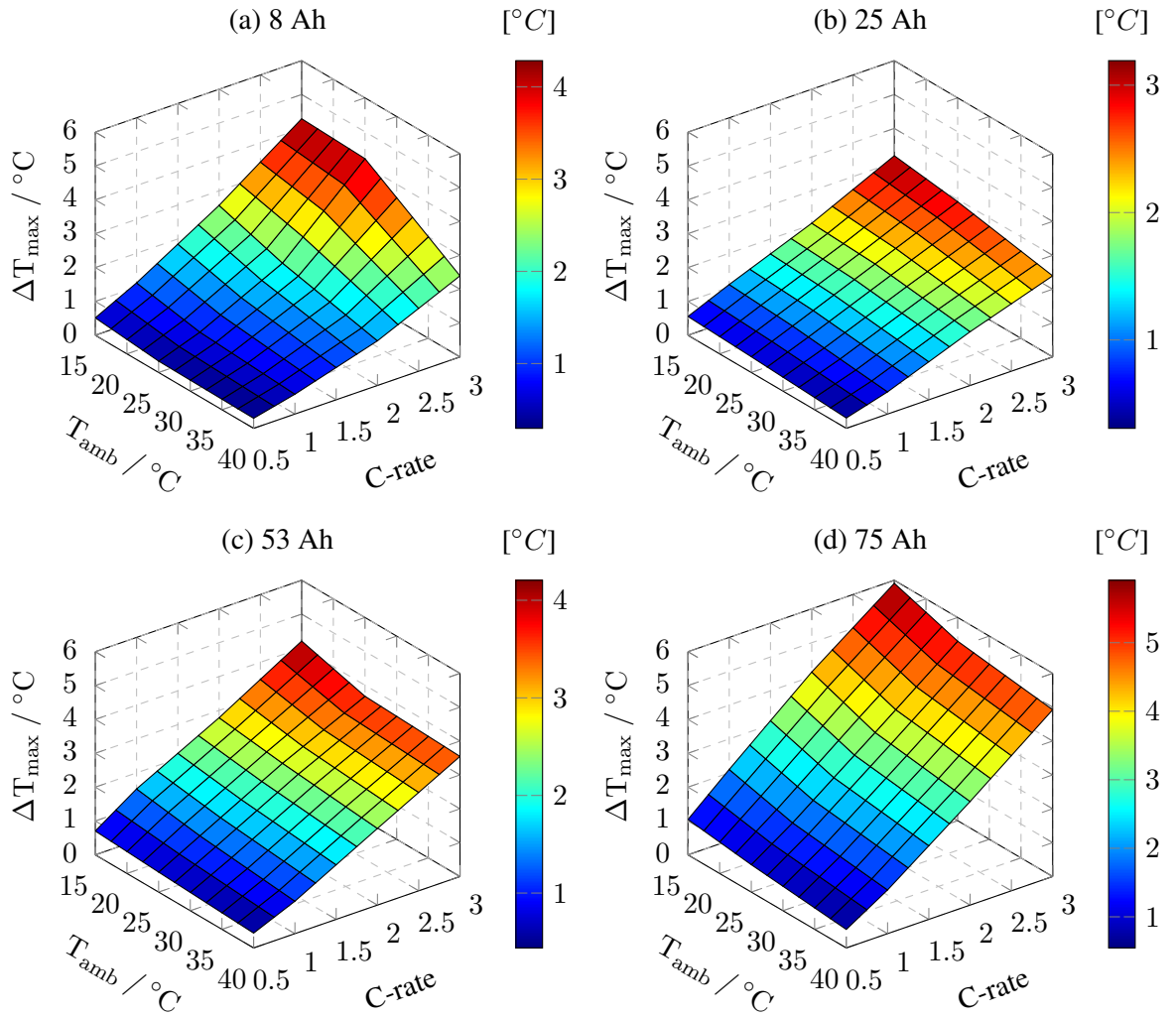

Figure 2: Maximum temperature gradient measured on cell surface, plotted versus c-rate and temperature

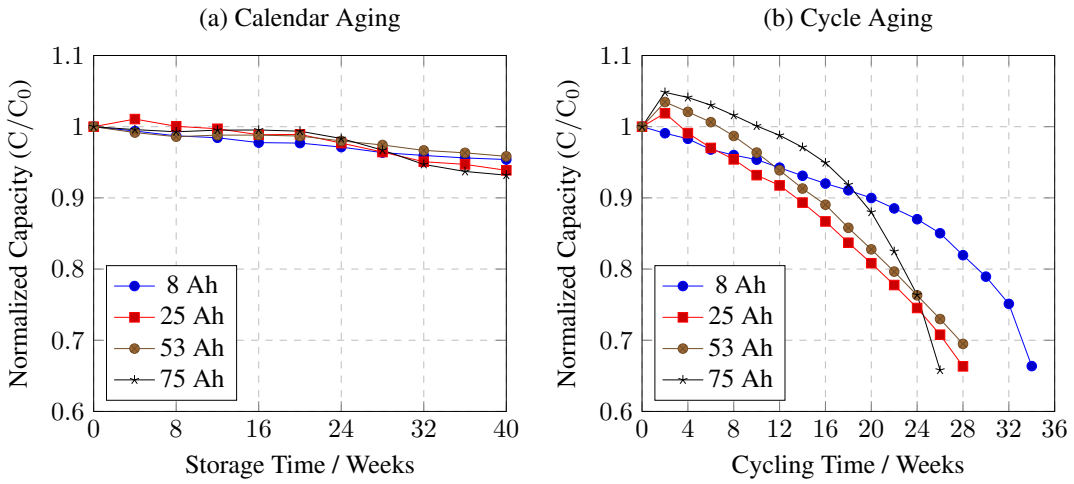

Figure 3: Plot of remaining capacity (normalized) for different cell size under calendar and cycle aging conditions

sults of cycle and calendar aging. It is a well established that calendar aging can be accelerated by high ambient temperature. Hence to obtain the aging results in a defined time frame, the conditions for calendar aging were set as 40°C and 100% SOC (i.e. the cells were fully charged before the storage).
Prior to the aging tests, the discharge capacity of the cells were measured at 100% SOC, 25°C and 1C discharge c-rate. The open circuit voltage (OCV) and hybrid pulse power characterization (HPPC) tests were performed as described in [14]. These tests can be collectively put together as reference performance test (RPT). The cells were then divided into two groups each for calendar and cycle aging tests. The aging tests were briefly interrupted at specific intervals, 4 weeks and 100 cycles for calendar and cycle aged cells respectively. During the brief interruption, the RPT is performed on the aged cells to obtain the aging parameters of cells such as remaining capacity, pulse power, impedance, OCV etc. After of the completion of this tests, the aging tests were continued until the remaining capacity of the cells fall below 70% of its nominal value or at the end of 40 weeks, whichever is earlier. In addition to these tests, long characterization were performed at every 12^{th} week and 400 cycles for calendar and cycle aged cells respectively. These tests include electrochemical impedance spectroscopy (EIS) test and one cycle of 0.05 C charge and discharge, a pseudo method to evaluate OCV of a given cell.

3 Results and Discussion

3.1 Capacity Fade

The cell discharge capacity was measured from a fully charged state (100% SOC) at 25°C and 1C discharge c-rate at the beginning of aging tests. These measurements were repeated at specific aging intervals after a brief pause in the aging tests, to calculate the capacity loss from the previous interval. Fig.3 shows the comparison of capacity fade during calendar and cycle aging tests for different cell sizes. These results clearly indicate that calendar aging has little influence on overall aging during the same period with cycle aging. In can be also observed that calendar aging is nearly same among different cell size, subject to $\pm 2\%$ variation in remaining capacity. The variation in the measurements can be contributed by multiple factors such as actual cell temperature, measurement inaccuracies, cell manufacturing conditions etc. But the fact remains that calendar aging has very little or no influence of cell size.
On the other hand, the results of cycle aged cells have a strong difference with the calendar aged cells. The evolution of capacity fade is highly nonlinear, i.e. the rate of capacity fade is not constant throughout the cycles. There is an increase in the cell capacity for most of the cells in the initial cycles, i.e between 0 to 2 weeks (2 weeks of cycling time corresponds to 100 cycles), except for 8 Ah cells. This is a strange phenomenon which has not been explained in literature related to aging studies. It could be related to additional formation effect. In general, capacity loss in the initial cycles is higher, which is mainly contributed by formation and growth of SEI layers. After the initial phase, the growth of SEI layer and consumption of cyclable lithium ions reduces [2, 15, 16]. Hence the rate of capacity loss decreases after few initial cycles. The 8 Ah cells show similar behavior to this.
Capacity balancing in lithium ion cells is done for optimal performance, as the gravimetric energy densities of electrode materials are different. They also have limited range of stoichiometry, in order to achieve reversible reaction or safety criteria. The product of these quantity provides the active mass of the electrode. The ratio of the active masses of anode and cathode are useful in the determination of capacity balancing of a cell as shown in Eq.(1).

$$\gamma = \frac{m_+}{m_-} = \frac{\Delta x C_-}{\Delta y C_+} \tag{1}$$

The notations Δx and Δy are the stiochiometric range of negative and positive electrodes, respectively. The electrode's active mass and coulombic capacity are denoted as m and C, respectively. In ideal conditions, the active mass ratio (γ) does not change over time and usage, i.e. constant capacity throughout. But in practical situations, there are many side reactions within the cell such as SEI layer formation, electrolyte decomposition, lithium plating and other aging processes etc. which causes distortion in the capacity balance. Hence optimized mass ratio is slightly higher than the ideal value in order to account of the side reactions [17]. In addition to this, anode capacity is slightly oversized with respect to cathode to prevent lithium plating on its surface.
Hence, the cell capacity increase in 25, 53 and 75 Ah cells can be explained by increased electrode area ratio (Tab.1) in comparison to 8 Ah cells. The additional cathode mass could have contributed to slight increase in the cell capacity in the initial stages. In the later stages, other side reactions contributed to the loss of cyclable lithium ions which resulted in the loss of capacity.
A closer look into Fig.3(b) reveals that there are stages where the capacity loss is linear with respect to cycling time, but it is not same for all cell types, indicating that size does have influence on aging. At the later stages of cycling the capacity loss becomes non linear towards the end of life (EOL). To get a better understanding of rate of capacity loss, the normalized discharged capacity was differentiated with respect to cycling time as shown in Fig. 4. The loss rate appears to be nearly constant for 8 Ah cells up to 24 weeks, this is also similar in 25 and 53 Ah cells, between 4 to 24 weeks of cycling time. However the 75 Ah cells showed increased rate of capacity loss throughout the cycling time. These results lead to the conclusion that, aging is not similar when cell sizing is taken into account and hence the in-

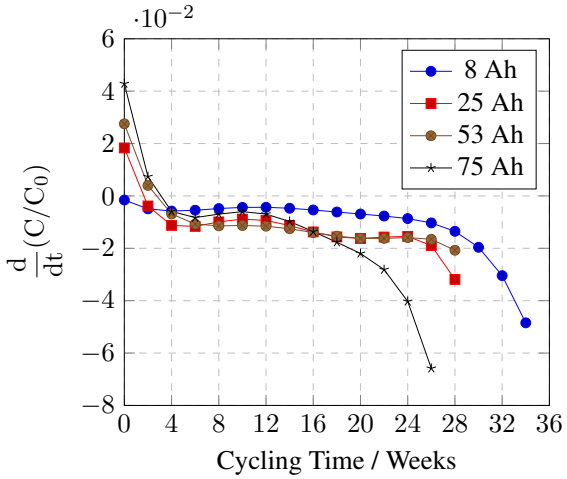

Figure 4: Plot of differential capacity fade with respect to cycling time

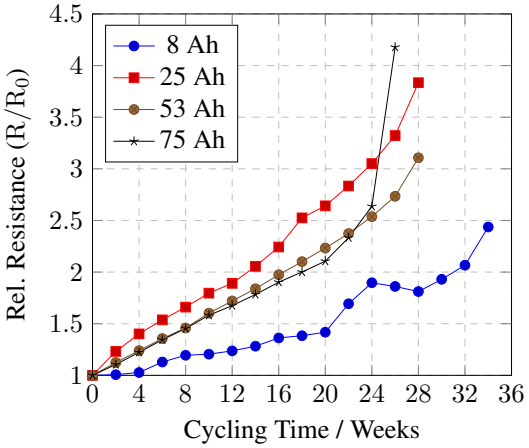

Figure 5: Normalized Resistance vs. cycle number of different cell size

crease in size has influence on cell aging which is strongly related to inhomogeneity.

3.2 Impedance Rise

Impedance rise is the result of aging in the cells which has contributions from ohmic drop, SEI layer, double layer capacitance, charge transfer reactions and diffusion of ions in the solid phase. The ohmic drop is contributed by the resistance of current collectors, active material, electrolyte, contact resistance etc. The SEI layers contributes to impedance rise due to its growth over time. A detailed analysis of the impedance rise can be done by performing EIS measurements at regular aging intervals. In the present work, the impedance rise is evaluated by performing high current DC pulse measurements and measuring the voltage response of the cell. The cell resistance is calculated as ratio of voltage response to current input as shown in Eq. (2).

$$R_{10s} = \left(\frac{\Delta V}{\Delta I} \right)_{t=10s} \tag{2}$$

Fig. 5 shows the plot of resistance for different cell size, calculated by 10 s high current pulse 3C discharge rate and normalized to its initial value. It can be seen that the rate of resistance increase is higher in 25, 53 and 75 Ah cells in comparison to 8 Ah cells. Resistance increase does not contribute directly to the loss of capacity, but it increases the voltage polarization thereby reaching the cut off voltage sooner. This is an indication of accelerated aging in large format cells. At 70% remaining capacity the resistance of 75 Ah cells is nearly doubled as that of 8 Ah cells. The rapid capacity loss is in relation to the resistance increase between 20 to 26 weeks.

3.3 Modeling

Based on the results of capacity loss and resistance increase, 75 Ah cells undergo faster degradation due to inhomogeneous aging. To investigate the cell inhomogeneity in relation to its size, multi dimensional multi physics models were built for 75 Ah cells in COMSOL Multiphysics platform. These models are very useful in the studying temperature, current density and voltage distribution within the cell. The schematic of this Multiphysics platform is shown in Fig. 6. The part (a) is the representation of 2 dimensional electrical model, depicting the electrical characteristics of the cell. This model is coupled with a 3 dimensional thermal model which evaluates the temperature distribution in the cell. The thermal model receives heat input from the electrical model and outputs the temperature to the electrical model and vice versa. The coupling between different coordinate system occurs as the variables are averaged over the model's geometry, thereby eliminating the coordinate system dependence. Then they are converted as surface or volumetric source terms into the models where they are used as inputs.
Fig. 6(b) shows the schematic of electrical model of a lithium ion pouch cell. In the actual cell, the components consists of current collectors, electrode materials for both positive and negative electrode and separator, together a they constitute a cell sandwich. To increase the cell capacity, many layers of cell sandwich are stacked up along the thickness direction of the cell. A single cell sandwich is shown here, represented by positive and negative current collectors (along XY plane) and transverse current density (J, along Z-direction) [10, 18]. The current collectors are shown in 2-D geometry, as the thickness is smaller compared to its length and width. The current flow in electrode materials and separator are assumed to be perpendicular as the distance between them is very small and they are collectively represented as J.
The electrical model is described by set of

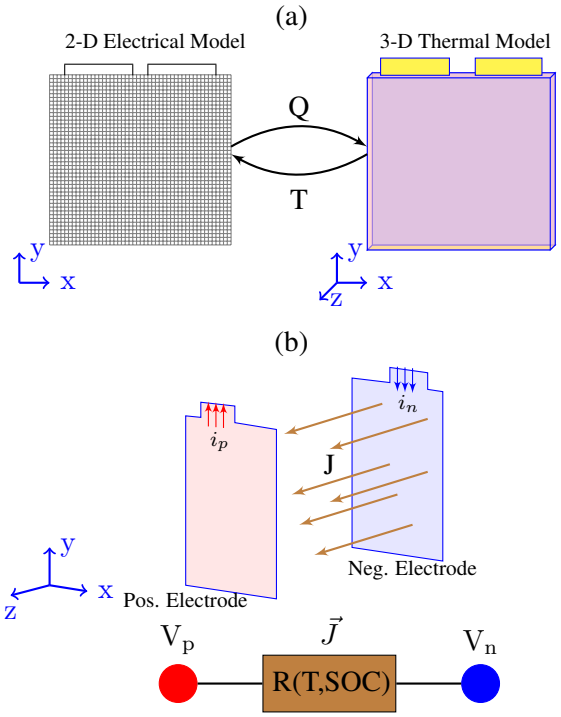

Figure 6: Schematic representation of 2-D electrical and 3-D thermal model

governing equations:

Eq. (3) describes the charge balance in the current collectors.

$$\sigma_j \frac{\partial^2 \Phi_j}{\partial x^2} + \sigma_j \frac{\partial^2 \Phi_j}{\partial y^2} + \frac{J \cdot \hat{u}}{\delta_j} = 0 \ \ (j = p, n) \quad (3)$$

Eqs. (4) and (5) are the boundary conditions at the interface between current collectors and tabs of positive and negative respectively.

$$\hat{u} \cdot (-\sigma_p \nabla \Phi_p) = \frac{I_{cell}}{L \delta_p} \quad (4)$$

$$\Phi_n = 0 \quad (5)$$

The remaining boundaries are assumed to be electrically insulated as represented in Eq. (6).

$$\hat{u} \cdot (\nabla \Phi_j) = 0 \ \ (j = p, n) \quad (6)$$

The transverse current density is calculated using Eq. (7).

$$J = \frac{U_{OCV} - (\Phi_p - \Phi_n)}{R \cdot L_j \cdot W_j} \quad (7)$$

The thermal model presented in this work is a simplified model. The cell electrode materials, electrolyte and separator are assumed to be made of one material, besides other components such as positive and negative current collectors and their respective tabs are included in the model development. This is done to reduce computational efforts and the model complexity without significant compromise on the accuracy of the model. The thermal model is described by the set of equations:

The energy conservation in the cell core is described by Eq. (8).

$$\rho C_p \frac{\partial T}{\partial t} = \frac{\partial}{\partial x}\left(\lambda_x \frac{\partial T}{\partial x}\right) + \frac{\partial}{\partial y}\left(\lambda_y \frac{\partial T}{\partial y}\right) + \frac{\partial}{\partial z}\left(\lambda_z \frac{\partial T}{\partial z}\right) + \dot{Q} \quad (8)$$

The heat source mainly comes from the cell over potential or ohmic drop during charge/discharge, this heat is also known as irreversible heat. This heat is dissipated in the cell irrespective of the direction of current flow. The second source of heat is the entropic heat or reversible heat. In addition to these, heat is dissipated due to current flow in the tabs and are described in Eqs. (9), (10) and (11).

$$\dot{Q} = q_{rev} + q_{irr} + q_{tabs} \quad (9)$$

$$q_{rev} = \frac{I_{cell}}{zF} \cdot T \cdot \Delta S \quad (10)$$

$$q_{irr} = I_{cell}^2 \cdot R \quad (11)$$

Heat flow also depends on the ambient temperature, if the cell temperature is different than ambient temperature, convective heat should be considered as shown in Eq. (12).

$$q_{conv} = h_{conv}(T - T_{ref}) \quad (12)$$

The thermal properties of the cell used in the model are shown in Tab. 2.

Table 2: Material properties of the cell used in the model

	ρ[kg m^{-3}]	C$_p$[J kg^{-1} K^{-1}]	λ[W m^{-1} K^{-1}]
Active Material [a]	1984.2	1438.8	{1.1667, 1.1667, 0.9196}
Positive tab [b]	2700	900	238
Negative tab [b]	8700	385	400
Outer foil [19]	1636	1377	0.427

3.4 Simulation Results

The models were simulated using the finite element method (FEM) tool developed by COMSOL Multiphysics, ver. 5.1. The 3-D thermal model was evaluated using the PARADISO (Parallel Direct Solver), whereas the 2-D electrical model was solved with MUMPS (Multifrontal

[a] Calculated
[b] Comsol Library

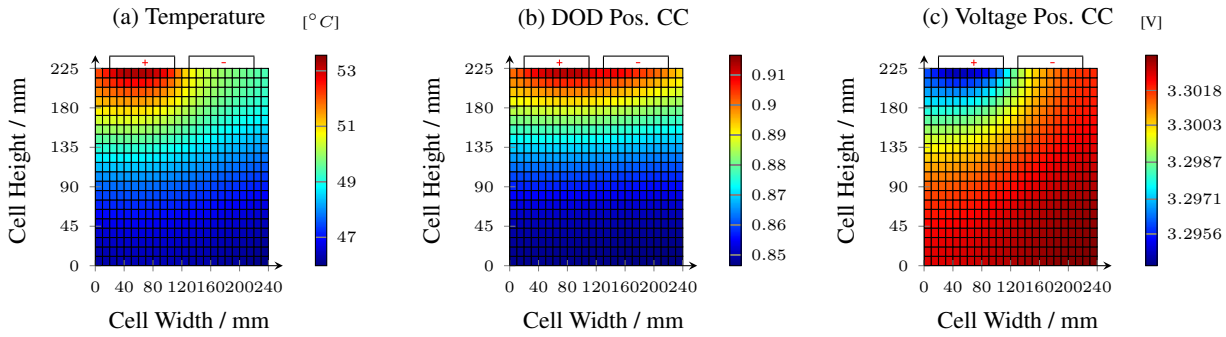

Figure 7: Surface distribution of (a) Temperature, (b) Depth of Discharge and (c) Voltage of type D cell during 3C discharge, $\mathrm{DOD}_{\mathrm{mean}}$ = 0.868 , 25°C ambient temperature

Massively Parallel Solver). Fig. 7 shows the plot of distribution of (a) surface temperature, (b) DOD on positive current collector and (c) voltage on positive current collector along the surface of 75 Ah cell. The simulation conditions were 3C discharge rate at 25°C ambient temperature. The experimental conditions were actually different from the simulation conditions because aging at 25°C is slower than at 40°C and cycling at 3C discharge rate requires stronger cooling to the cells, which were not implemented during the aging tests. These Multiphysics simulations provide endless combinations of tests conditions with varying temperature and c-rates, at the cost of high computation and with the benefit of time, experimental cost and no safety risks as experienced during test conditions. Also, the operating conditions of EV batteries in real life conditions are similar to the simulation conditions i.e. 25°C ambient temperature and 3C discharge rate.

The snapshot of the surface distribution was taken at DOD = 0.868 (based on Ah-counting). It can be seen that temperature distribution is not uniform along the in-plane (XY) direction of the cell. The ΔT on the surface is $\approx$ 6°C. Hot stops can be seen at the vicinity of positive tab and the more cooler regions are at the coordinates farthest from the tabs. The positions near the tab experience high current density, as this is the path of entry and exit of the currents. However the negative tab appears to be slightly cooler than the positive tab, this could be due to different material properties of the current collectors and their respective tabs.

The DOD profile along the surface shows similar distribution near the tabs, where there is a higher DOD near the tabs compared to other coordinates along the surface. Since DOD is the measure of discharge level in the cell, the positions near the tabs undergo more discharge compared to other locations. This could lead to over discharge when the cell is completely discharged, as it can be seen that when the positions near tabs has DOD $\approx$ 0.91, the mean DOD was only 0.868. Similar profile can be seen to the voltage distribution on the positive current collector.

By observing these surface distribution, it is clear that the position near the cell tabs undergo severe stress in the form of temperature, current and voltage that lead to accelerated aging. It is well known from the Arrhenius relations of the temperature, every 10°C increase could lead to nearly doubling of the cell aging as shown in Eq. (13). Where A(T) is the aging factor, A_0 is the initial factor, E_a is the activation energy, T is cell temperature (K).

$$A(T) = A_0 \cdot exp\left(\frac{-E_a}{RT}\right) \tag{13}$$

The effects of current and voltage on accelerated aging can be similarly expressed by exponential functions [20, 21]. If a cell is subjected to these inhomogeneities over longer period, the active materials near the tabs undergo faster degradation and positions away the tabs experiences slower degradation. This causes localized aging within the cell and creates a region of weaker and stronger sub cells. The weaker sub cells with lower capacity and higher internal resistance exhibit higher over potential locally in comparison to stronger sub cells. These weaker cells are further degraded by higher local temperature and DOD. The effects of inhomogeneous aging could also lead to non uniform utilization of the active material, due to higher over potential on the weaker sub cells, the cut off voltage is reached sooner and the full capacity of the cell will not be used.

4 Conclusion

In this paper, the aging characterization of commercial lithium ion cells of NMC chemistry were studied with respect to their cell size. The cells of different sizes were subjected to calendar and cycle aging at 40°C ambient temperature. The results showed that cell inhomogeneities (temperature, current distribution and SOC) are influenced by sizing, i.e. larger cell size leads to increased inhomogeneity in the cell. The aging test results validates that inhomogeneity occurs mainly due to cycling conditions and aging is similar during storage conditions irrespective of the cell size.

The capacity fade evolution under cycling aging conditions is nonlinear across different sizes. The non linearity is greater in 75 Ah cells, where

it was observed to have steep capacity loss between weeks 20 and 26. Other cell sizes showed different rate of capacity loss, which is nearly constant until they experienced steep capacity loss towards their EOL. The impedance rise in the cells, another aging characteristic showed steep rise in the 75 Ah cells towards its EOL. These results lead to conclusion that, aging is not similar for all cell sizes and it is strongly related to inhomogeneity within a cell.
The cell inhomogeneity in 75 Ah cell was investigated using coupled electrical and thermal model. The simulation results showed varying degree of inhomogeneity within the cell. The positions near the cell tabs experienced additional stresses in the form of temperature, current and voltage distribution with respect to locations farthest from the tabs. A long term exposure of these operational stresses lead to localized or inhomogeneous aging within the cell and may cause premature EOL of the cell [22–24]. Further tests are necessary to confirm these findings, such as measuring temperature gradient in aged cells and comparing them with the fresh cells across different cell size. Postmortem analyses of cells could reveal the extend of localized degradation within the cell.

List of symbols

σ_j Electrical conductivity of the current collector / S m^{-1}

Φ_j Voltage distribution in current collector / V

δ_j Thickness of current collector / m

$\hat{u}$ Unit vector indicating the direction of J

L Width of the tab / m

I_{cell} Input current / A

U_{OCV} Open circuit voltage / V

R Cell resistance / Ω

L_j Length of the electrode material / m

W_j Width of the electrode material / m

ρ Density / kg m^{-3}

C_p Specific heat capacity / J kg^{-1} K^{-1}

λ Thermal conductivity / W m^{-1} K^{-1}

$\dot{Q}$ Heat generation / W m^{-3}

ΔS Entropic heat coefficient / J K^{-1} mol^{-1}

F Faraday number = 96485.33 C

z Stiochiometric coefficient = 1 for Li

h_{conv} Convective heat coefficient = 5 W m^{-2} K^{-1}

T_{ref} the ambient temperature / K

x, y, z Values along x-, y-, and z-directions respectively

Acknowledgment

This work has been done in the framework of CREATE research programme funded by the Singapore National Research Foundation (NRF).

References

[1] Y. Zhang and C.-Y. Wang, "Cycle-life characterization of automotive lithium-ion batteries with $LiNiO_2$ cathode," *Journal of the Electrochemical Society*, vol. 156, no. 7, pp. A527–A535, 2009. [Online]. Available: http://dx.doi.org/10.1149/1.3126385

[2] A. Barré, B. Deguilhem, S. Grolleau, M. Gérard, F. Suard, and D. Riu, "A review on lithium-ion battery ageing mechanisms and estimations for automotive applications," *Journal of Power Sources*, vol. 241, pp. 680–689, 2013. [Online]. Available: http://dx.doi.org/10.1016/j.jpowsour.2013.05.040

[3] M. Kassem, J. Bernard, R. Revel, S. Pelissier, F. Duclaud, and C. Delacourt, "Calendar aging of a graphite/$LiFePO_4$ cell," *Journal of Power Sources*, vol. 208, pp. 296–305, 2012. [Online]. Available: http://dx.doi.org/10.1016/j.jpowsour.2012.02.068

[4] J. Belt, V. Utgikar, and I. Bloom, "Calendar and phev cycle life aging of high-energy, lithium-ion cells containing blended spinel and layered-oxide cathodes," *Journal of Power Sources*, vol. 196, no. 23, pp. 10 213–10 221, 2011. [Online]. Available: http://dx.doi.org/10.1016/j.jpowsour.2011.08.067

[5] J. Vetter, P. Novák, M. Wagner, C. Veit, K.-C. Möller, J. Besenhard, M. Winter, M. Wohlfahrt-Mehrens, C. Vogler, and A. Hammouche, "Ageing mechanisms in lithium-ion batteries," *Journal of power sources*, vol. 147, no. 1, pp. 269–281, 2005. [Online]. Available: http://dx.doi.org/10.1016/j.jpowsour.2005.01.006

[6] M. Broussely, P. Biensan, F. Bonhomme, P. Blanchard, S. Herreyre, K. Nechev, and R. Staniewicz, "Main aging mechanisms in li ion batteries," *Journal of power sources*, vol. 146, no. 1, pp. 90–96, 2005. [Online]. Available: http://dx.doi.org/10.1016/j.jpowsour.2005.03.172

[7] G. Ning, R. E. White, and B. N. Popov, "A generalized cycle life model of rechargeable li-ion batteries," *Electrochimica acta*, vol. 51, no. 10, pp. 2012–2022, 2006. [Online]. Available: http://dx.doi.org/10.1016/j.electacta.2005.06.033

[8] S. F. Schuster, T. Bach, E. Fleder, J. Müller, M. Brand, G. Sextl, and A. Jossen, "Nonlinear aging characteristics of lithium-ion cells under different operational conditions," *Journal of Energy Storage*, vol. 1, pp. 44–53, 2015. [Online]. Available: http://dx.doi.org/10.1016/j.est.2015.05.003

[9] G.-H. Kim, K. Smith, K.-J. Lee, S. Santhanagopalan, and A. Pesaran, "Multi-domain modeling of lithium-ion batteries encompassing multi-physics in varied

length scales," *Journal of The Electrochemical Society*, vol. 158, no. 8, pp. A955–A969, 2011. [Online]. Available: http://dx.doi.org/10.1149/1.3597614

[10] P. Taheri, A. Mansouri, B. Schweitzer, M. Yazdanpour, and M. Bahrami, "Electrical constriction resistance in current collectors of large-scale lithium-ion batteries," *Journal of The Electrochemical Society*, vol. 160, no. 10, pp. A1731–A1740, 2013. [Online]. Available: http://dx.doi.org/10.1149/2.041310jes

[11] P. Osswald, S. Erhard, J. Wilhelm, H. Hoster, and A. Jossen, "Simulation and measurement of local potentials of modified commercial cylindrical cells i. cell preparation and measurements," *Journal of The Electrochemical Society*, vol. 162, no. 10, pp. A2099–A2105, 2015. [Online]. Available: https:/dx.doi.org/10.1149/2.0561510jes

[12] S. V. Erhard, P. J. Osswald, J. Wilhelm, A. Rheinfeld, S. Kosch, and A. Jossen, "Simulation and measurement of local potentials of modified commercial cylindrical cells," *Journal of The Electrochemical Society*, vol. 162, no. 14, pp. A2707–A2719, 2015. [Online]. Available: https:/dx.doi.org/10.1149/2.0431514jes

[13] C. Veth, D. Dragicevic, and C. Merten, "Thermal characterizations of a large-format lithium ion cell focused on high current discharges," *Journal of Power Sources*, vol. 267, pp. 760–769, 2014. [Online]. Available: http://dx.doi.org/10.1016/j.jpowsour.2014.05.139

[14] R. Arunachala, K. Makinejad, S. Athlekar, A. Jossen, and J. Garche, "Cycle life characterisation of large format lithium-ion cells," in *Electric Vehicle Symposium and Exhibition (EVS27), 2013 World*. IEEE, 2013, pp. 1–9. [Online]. Available: http://dx.doi.org/10.1109/EVS.2013.6914865

[15] M. Dubarry, C. Truchot, and B. Y. Liaw, "Synthesize battery degradation modes via a diagnostic and prognostic model," *Journal of power sources*, vol. 219, pp. 204–216, 2012. [Online]. Available: http://dx.doi.org/10.1016/j.jpowsour.2012.07.016

[16] D. Liu, Y. Wang, Y. Xie, L. He, J. Chen, K. Wu, R. Xu, and Y. Gao, "On the stress characteristics of graphite anode in commercial pouch lithium-ion battery," *Journal of Power Sources*, vol. 232, pp. 29–33, 2013. [Online]. Available: http://dx.doi.org/10.1016/j.jpowsour.2012.12.110

[17] P. Arora, R. E. White, and M. Doyle, "Capacity fade mechanisms and side reactions in lithium-ion batteries," *Journal of the Electrochemical Society*, vol. 145, no. 10, pp. 3647–3667, 1998. [Online]. Available: http://dx.doi.org/10.1149/1.1838857

[18] B. Wu, Z. Li, and J. Zhang, "Thermal design for the pouch-type large-format lithium-ion batteries i. thermo-electrical modeling and origins of temperature non-uniformity," *Journal of The Electrochemical Society*, vol. 162, no. 1, pp. A181–A191, 2015. [Online]. Available: http://dx.doi.org/10.1149/2.0831501jes

[19] S. Du, M. Jia, Y. Cheng, Y. Tang, H. Zhang, L. Ai, K. Zhang, and Y. Lai, "Study on the thermal behaviors of power lithium iron phosphate (lfp) aluminum-laminated battery with different tab configurations," *International Journal of Thermal Sciences*, vol. 89, pp. 327–336, 2015. [Online]. Available: http://dx.doi.org/10.1016/j.ijthermalsci.2014.11.018

[20] J. Wang, P. Liu, J. Hicks-Garner, E. Sherman, S. Soukiazian, M. Verbrugge, H. Tataria, J. Musser, and P. Finamore, "Cycle-life model for graphite-$LiFePO_4$ cells," *Journal of Power Sources*, vol. 196, no. 8, pp. 3942–3948, 2011. [Online]. Available: http://dx.doi.org/10.1016/j.jpowsour.2010.11.134

[21] M. Ecker, J. B. Gerschler, J. Vogel, S. Käbitz, F. Hust, P. Dechent, and D. U. Sauer, "Development of a lifetime prediction model for lithium-ion batteries based on extended accelerated aging test data," *Journal of Power Sources*, vol. 215, pp. 248–257, 2012. [Online]. Available: http://dx.doi.org/10.1016/j.jpowsour.2012.05.012

[22] A. Awarke, S. Pischinger, and J. Ogrzewalla, "Pseudo 3d modeling and analysis of the sei growth distribution in large format li-ion polymer pouch cells," *Journal of the Electrochemical Society*, vol. 160, no. 1, pp. A172–A181, 2013. [Online]. Available: http://dx.doi.org/10.1149/2.022302jes

[23] M. Fleckenstein, O. Bohlen, M. A. Roscher, and B. Bäker, "Current density and state of charge inhomogeneities in li-ion battery cells with lifepo 4 as cathode material due to temperature gradients," *Journal of Power Sources*, vol. 196, no. 10, pp. 4769–4778, 2011. [Online]. Available: http://dx.doi.org/10.1016/j.jpowsour.2011.01.043

[24] C. Veth, D. Dragicevic, R. Pfister, S. Arakkan, and C. Merten, "3d electro-thermal model approach for the prediction of internal state values in large-format lithium ion cells and its validation," *Journal of The Electrochemical Society*, vol. 161, no. 14, pp. A1943–A1952, 2014. [Online]. Available: http://dx.doi.org/10.1149/2.1201412jes

Authors

Raghavendra Arunachala earned his B.Eng. in electrical and electronic engineering from Visveswaraya Technological University, India. He completed his M.Sc from Rheinische Westflische Technische Hochschule (RWTH) Aachen University, Germany in 2011. He is currently a doctoral student in TUM CREATE, Singapore, working in the area of electrical energy storage systems.

Lemuel Moraleja earned his Bachelors Degree in Electronics Engineering from University of the Philippines Diliman, Philippines in 2010. He is currently the Laboratory Manager for the Energy Storage Systems Laboratory in TUM CREATE, Singapore.

Andreas Jossen earned his doctorate, dealing with “Management of photo-voltaic plants using energy storage systems”at University of Stuttgart. From 1994 he was group leader for different battery related topics with ZSW, Ulm. Since 2010 he is full professor at the Institute for Electrical Energy Storage Technology, TUM.

Juergen Garche received his PhD and habilitation (post-doctoral lecturing qualification) in theoretical and applied electrochemistry at Dresden University of Technology. He is dealing since $>$ 40 years with batteries and fuel cells. He build up the ZSW Ulm as director. Now he managed the Fuel Cell and Battery consulting office FCBAT.